January 2009

A phenomenological discrete brittle damage-mechanics model for fatigue of MEMS devices with application to LIGA Ni

T. S. Slack

F. Sadeghi

D. Peroulis

Slack, T. S.; Sadeghi, F.; and Peroulis, D., "A phenomenological discrete brittle damage-mechanics model for fatigue of MEMS devices with application to LIGA Ni" (2009). *Department of Electrical and Computer Engineering Faculty Publications.* Paper 62.
http://dx.doi.org/http://dx.doi.org/10.1109/JMEMS.2008.2008064

A Phenomenological Discrete Brittle Damage-Mechanics Model for Fatigue of MEMS Devices With Application to LIGA Ni

Trevor S. Slack, Farshid Sadeghi, *Fellow, ASME*, and Dimitrios Peroulis

***Abstract*—Fatigue initiation and failure of various microelectromechanical systems (MEMS) is of significant importance as they gain widespread acceptance in sensors and electronics. This paper presents an approach for utilizing available experimental fatigue data to evaluate the fatigue lives of MEMS components. The approach is based on a phenomenological discrete material representation in which a domain is represented by a collection of rigid elements that interacts via springs along their boundaries. The principles of continuum damage mechanics are used to degrade the spring stiffnesses as brittle damage occurs when the domain is subjected to fatigue loading. The model utilizes experimental stress–life data for LIGA Ni to identify the material properties used in the model. The proposed model captures the statistical distribution of material properties and geometrical randomness of the microstructure commonly observed in a wide variety of MEMS. Consequently, simulations that account for the variability in fatigue life can be readily performed. The model is applied to a dog-bone-shaped specimen to evaluate the influence of material heterogeneity and material flaws on fatigue crack initiation life and scatter. The ability of the model to predict the fatigue life of different types of MEMS devices and loading conditions is also demonstrated by simulating the fatigue stress–life behavior of a MEMS resonator support beam. [2008-0087]**

***Index Terms*—Damage mechanics, discrete-element method, fatigue, microelectromechanical systems (MEMS).**

I. Introduction

THE APPLICATIONS of microelectromechanical systems (MEMS) are continuously growing. The successful development of a device requires both the experimental determination of relevant material properties as well as modeling techniques that can capture heterogeneous effects caused by the material microstructure. In many applications such as accelerometers [1], angular rate sensors [2] and RF MEMS switch and varactor [3] components are subjected to cyclically varying loads and are expected to withstand billions or trillions of loading cycles. In other applications, the MEMS device may be subjected to unwanted machine vibrations. For this reason, it is important to understand the fatigue behavior of materials used in MEMS devices.

The mechanical performance of materials used in MEMS devices depends both on the fabrication process and post-processing [4]. Thus, to accurately measure the mechanical properties of MEMS devices, experiments have to be performed on micrometer-scale specimens. Much of the work in fatigue characterization has been conducted for polysilicon due to its predominant use as a structural material for MEMS. Various approaches have been attempted using both integrated and external actuations of specimens in bending and tension [5]–[8]. A review of the test devices developed, as well as a comparison of the experimental data obtained by different research groups for polysilicon, has been compiled by Sharpe and Bagdahn [9]. The results presented by Sharpe and Bagdahn [9] show significant discrepancy between the results from different groups and a large amount of scatter in the results for each group. Several fatigue mechanisms have been proposed, including stress-assisted surface oxide dissolution, reaction layer fatigue, and mechanically induced subcritical cracking [10].

Significant work has also been done to characterize the fatigue behavior of LIGA Ni [11]–[14]. Yang *et al.* [13] performed tensile testing of samples composed of both columnar and nanoscale grains. Depending on the thickness of the samples with columnar grains, fatigue behavior was observed to be similar to either annealed Ni or wrought Ni. A significant strengthening of fatigue resistance was found for the samples with nanoscale grains. The samples with columnar grains showed evidence of persistent slip bands at which cracks were often found to nucleate. For the nanostructured samples, cracks were found to nucleate from pre-existing surface and corner defects. Aktaa *et al.* [12] also performed direct tensile testing of LIGA Ni. By extending their results to the fully reversed loading condition, they also found a good comparison with fatigue properties of bulk Ni. Boyce *et al.* [14] performed fully reversed fatigue testing on coarse-grained LIGA Ni bending specimens. They also found behavior similar to bulk Ni. They presented evidence of fatigue-induced microcracking and cracks propagating intergranularly from surface oxides. They discovered a fatigue-driven surface oxidation mechanism wherein the growth of persistent slip bands disrupts the native passivation oxide layer, allowing for the growth of a brittle oxide layer hundreds of times thicker than the native oxide layer which then acts as a site for crack nucleation.

Manuscript received April 1, 2008; revised October 1, 2008. First published December 22, 2008; current version published February 4, 2009. This work was supported by the DARPA MEMS/NEMS S&T Fundamentals Program through the IMPACT Center. Subject Editor S. M. Spearing.

T. S. Slack and F. Sadeghi are with the School of Mechanical Engineering, Purdue University, West Lafayette, IN 47906 USA (e-mail: tslack@purdue.edu).

D. Peroulis is with the School of Electrical and Computer Engineering, Purdue University, West Lafayette, IN 47906 USA.

Color versions of one or more of the figures in this paper are available online at http://ieeexplore.ieee.org.

Digital Object Identifier 10.1109/JMEMS.2008.2008064

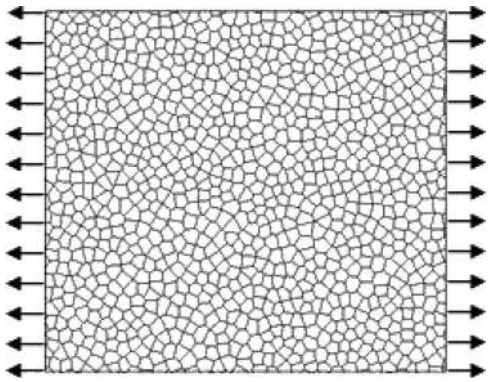

Fig. 1. Solid formed by a collection of discrete elements subjected to an applied external boundary loading.

This paper presents a modeling approach which utilizes available experimental results in a way that allows for the stochastic fatigue modeling of MEMS devices. The model is based on the theory of damage mechanics [15]–[17] and explicitly takes into account the gradual material degradation that occurs under cyclic loading. The methodology consists of solving the coupled damage evolution and material constitutive equations in a discrete material framework that accounts for the stochastic nature of the material microstructure and properties. The model is applied to a dog-bone-shaped tensile specimen to evaluate the influence of various material parameters and randomness of grain boundary structure on fatigue scatter. Initial material flaws such as broken bonds and voids are then randomly introduced into the dog-bone specimen to investigate their effects on fatigue life and fatigue life scatter. Finally, the model is used to predict the lifetime of a MEMS resonator support bracket.

II. Discrete Element Material Representation

The analysis presented in this investigation is based on a discrete material representation. The method differs from the standard numerical techniques such as the finite element method where a domain is discretized into smaller subdomains in order to integrate the governing equations derived from continuum mechanics. In the discrete element method, a domain is composed of smaller subdomains that interact with one another through contact at their boundaries. This is illustrated in Fig. 1 which shows a material domain that is composed of numerous interacting microelements that represent, in this case, the grains of the material. Each element is a rigid body with two translational degrees of freedom and one rotational degree of freedom. The elements are connected along their lines of intersection with a continuous set of fibers. As shown in Fig. 2(a), as one element moves relative to another, the fibers connecting the two elements are stretched. The stretching of the fiber results in forces between the two elements. As shown in Fig. 2(b), the forces are decomposed into normal and tangential components and are given both elastic and viscous properties. For the current study, only elastic effects are considered with fiber stiffnesses, K_n in the normal direction and K_t in the tangential direction, that are related to the macroscopic elastic properties E (modulus of elasticity) and ν (Poisson's ratio) [18]. The interaction of an element with all of its neighbors

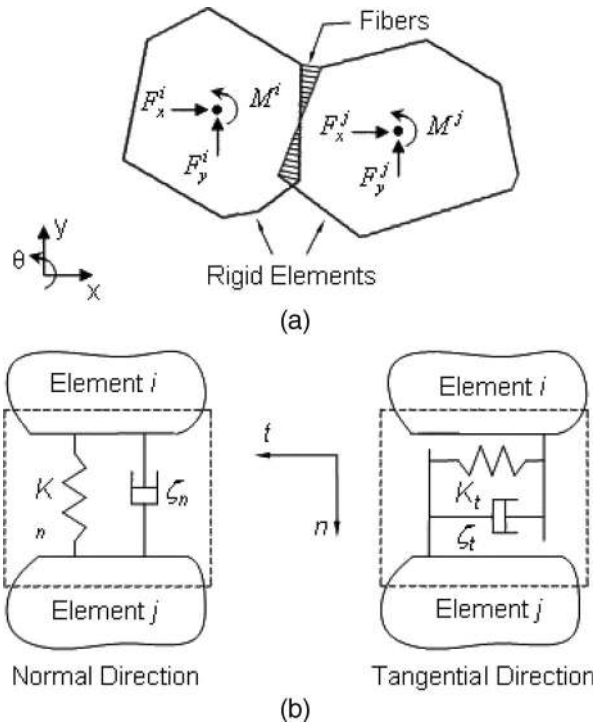

Fig. 2. (a) Interelement contact in the discrete model. (b) Fiber model.

results in an equivalent force $\boldsymbol{F}$ and moment $\boldsymbol{M}$ being applied to the element's center of mass. The solution of a given boundary value problem consists of specifying the time-dependent boundary conditions and the simultaneous integration of the equations of motion for all the elements in the domain. Further details of the element interaction and the method by which stresses are extracted can be found in [18] and [19].

The grains of a polycrystalline material can be represented to a good degree of accuracy through the process of Voronoi tessellation [20], [21]. This process consists of using a set of randomly placed points as nucleation points or seeds and constructing regions around them such that all points enclosed by the region are closer to the given nucleation point than any other nucleation point. The process results in a set of convex polygons known as Voronoi polygons. The randomly placed nucleation points lead to a nonunique material domain for every tessellation simulation. This produces topological randomness in the simulated microstructures. In the present model, the microelements are taken to be material grains that are generated through such a Voronoi tessellation process. The size of the grains is controlled by specifying the density of the nucleation points. The generated element shapes have variable number of sides and variable orientations. The most probable number of sides is six, which also corresponds to the number of sides for maximum thermodynamic stability of material grains. Care is taken during the tessellation process to obtain uniformity of the grain size by setting upper and lower limits on the distances between the nucleation points.

III. Fatigue Damage Modeling

Damage mechanics is concerned with the progressive deterioration of a material due to the initiation and growth of

microcracks and voids [15]–[17], [22]. The initiation and early growth of damage is discontinuous and is strongly affected by the heterogeneous nature of polycrystalline materials [23]. The effects of damage on the mechanical response of a material are captured through the introduction of a damage variable D into the constitutive equations. In general, the damage variable is a tensor, but under the assumption of isotropic damage, it reduces to a scalar variable D. A 1-D damaged coupled elasticity law takes the form

$$\sigma = (1 - D)E\varepsilon \tag{1}$$

where the value of D ranges from zero for an undamaged material to one for a completely damaged material. A value of one corresponds to a complete loss of stiffness in tension signifying crack initiation.

Constitutive equations for the evolution of the damage variable have been formulated within the framework of thermodynamics for fatigue damage, ductile damage, and creep damage [22]. For high-cycle fatigue, a commonly used form for the evolution of D which assumes a brittle damage mechanism is [24]–[27]

$$\frac{dD}{dN} = \left[\frac{\sigma_a}{\sigma_r(\sigma_m) \times (1 - D)}\right]^m \tag{2}$$

where N is the cycle number, σ_a is the stress amplitude, σ_m is the mean stress, and σ_r and m are temperature-dependent material parameters that have to be experimentally identified. Note that the term $\sigma_r(\sigma_m)$ is a function giving the dependence of the material parameter on σ_r mean stress. This material parameter is also referred to as the resistance stress [27], so called because it is the parameter that controls an element's ability to resist damage accumulation. The damage variable is implemented within the current modeling framework through the reduction of the fiber stiffness components as

$$\begin{aligned}(K_n) &= (K_n)^0(1 - hD)\\ (K_t) &= (K_t)^0(1 - hD)\end{aligned} \tag{3}$$

where $(K_n)^0$ and $(K_t)^0$are the initial normal and tangential stiffness components and h is a crack closure parameter. The crack closure parameter is introduced to capture the effects of the partial closing of microcracks that occur in compression. The value of h is one in tension and, following Lemaitre [22], is taken as 0.2 in compression. The effect of damage on the normal stress–strain relationship for a particular joint, including the crack closure effect, is shown in Fig. 3.

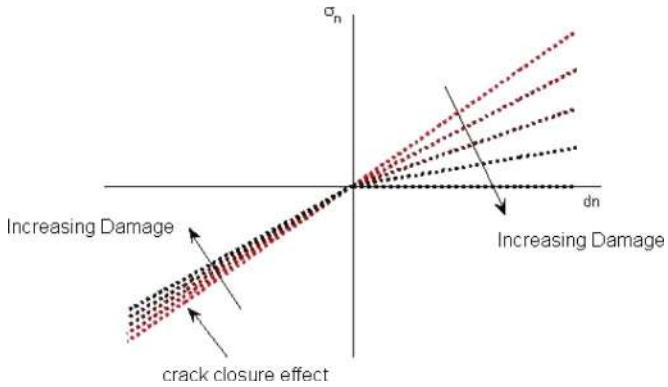

Fig. 3. Degradation of joint normal stiffness with damage accumulation.

IV. Numerical Solution of the Damaged Coupled Equations

The fatigue simulation is carried out by applying (2) locally to every element-to-element fiber set within the material domain. Solution of the resulting system of coupled first-order differential equations requires knowledge of the stress amplitude σ_a in every fiber set as a function of the fatigue cycle N. Since high-cycle fatigue involves millions of cycles, a fully coupled analysis using the material model is impossible and a compromise has to be made. The procedure adopted here is referred to as the "jump-in-cycles" method and is outlined by Lemaitre [22].

The method assumes a piecewise periodic loading that is constant over a number of cycles N^i during which the damage of all the interelement joints is known to be D_j^i, where j ranges over the number of joints in the domain and i indicates a block of cycles. The material model is used to determine the stress amplitude $(\sigma_a)_j^i$ in the joints, and the damage evolution rate in each joint is given by

$$\left(\frac{dD}{dN}\right)_j^i = \left[\frac{(\sigma_a)_j^i}{\sigma_r(\sigma_m) \times (1 - D_j^i)}\right]^m. \tag{4}$$

The increment in damage ΔD is assumed to be constant over the block of cycles, so the number of cycles in the current block of cycles is computed as

$$\Delta N^i = \frac{\Delta D}{\left(\frac{dD}{dN}\right)_{\text{crit}}^i} \tag{5}$$

where

$$\left(\frac{dD}{dN}\right)_{\text{crit}}^i = \text{Max}\left|\left(\frac{dD}{dN}\right)_j^i\right| \tag{6}$$

is the joint with the maximum damage evolution rate. The number of cycles is updated as

$$N^{i+1} = N^i + \Delta N^i \tag{7}$$

and the damage at each joint is updated using

$$D_j^{i+1} = D_j^i + \left(\frac{dD}{dN}\right)_j^i \Delta N^i. \tag{8}$$

The joint fiber stiffnesses are updated according to (3), and the procedure is repeated for the next block of cycles. The value of the damage increment ΔD has to be chosen large enough to allow a reasonable computational time but small enough so that the coupling between damage and stress is not violated. The piecewise linear growth in damage produced by the procedure is shown in Fig. 4.

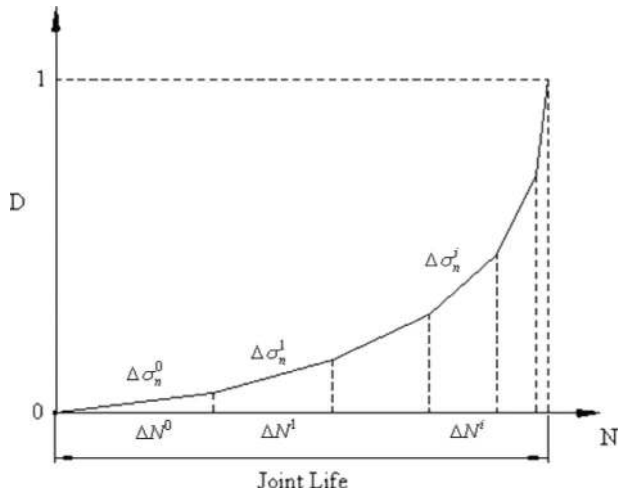

Fig. 4. Piecewise-linear approximation for damage evolution.

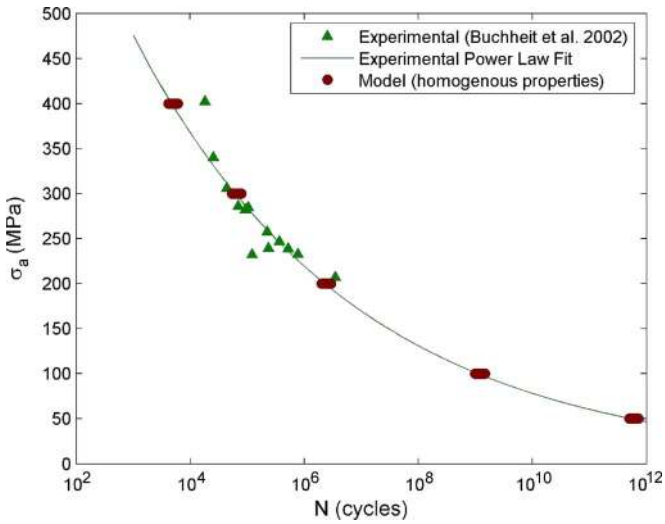

Fig. 5. S–N curve for LIGA Ni [11].

V. Identification of Material Fatigue Parameters

As described earlier, the fatigue damage evolution equation introduces two new material parameters that have to be experimentally determined. Direct measurement of the evolution of the damage variable is a destructive process that would require measurement of the total crack area on the surface of specimens that have been fatigued at different numbers of cycles. Indirect methods can also be used in which damage is measured via its effect on some measurable quantity such as stress amplitude, elastic modulus, or electrical resistance [22]. Given the limited amount of currently available experimental data, the method used here is to identify the parameters from experimental stress–life data (S–N curve) available in the literature. Buchheit *et al.* [11] performed fully reversed, $R = -1$, evaluation of LIGA Ni samples. Their experimental results are shown in Fig. 5. Also shown is a power law fit of the data of the form

$$\sigma_a = aN^b \tag{9}$$

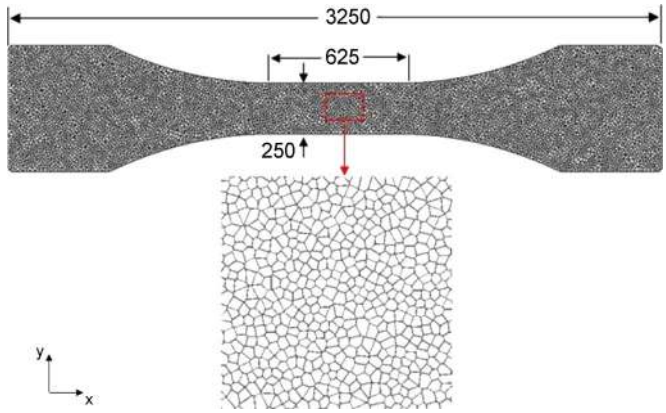

Fig. 6. Fatigue specimen modeled using the discrete-element-based material model. Dimensions are given in micrometers.

where σ_a is the stress amplitude. By using the least squares method, the curve fit parameters to the experimental results are determined to be

$$a = 1031\ \text{MPa} \quad b = -0.112. \tag{10}$$

To identify the material fatigue parameters, the damage evolution equation is integrated from the undamaged to the completely damaged states by assuming that there is no coupling between the damage variable and stress level, giving

$$\int_0^{N_f} dN = \int_0^1 \left\{ \frac{\sigma_r^*(1-D)}{\sigma_a} \right\}^m dD \Rightarrow N_f = \frac{1}{(m+1)} \left[\frac{\sigma_r^*}{\sigma_a} \right]^m \tag{11}$$

where N_f is the number of cycles to failure at the stress amplitude σ_a and σ_r^* is the value of the resistance stress under the fully reversed stress condition. When a nonzero mean stress is considered, an additional material parameter is introduced through the function $\sigma_r(\sigma_m)$ that would require additional experimental data at a different mean stress level to identify (for an example, see [25]). Rearranging (11) gives

$$\sigma_a = \sigma_r^*(m+1)^{-\frac{1}{m}} N^{-\frac{1}{m}}. \tag{12}$$

A comparison of (12) with (9) and (10) gives the fatigue material parameters as

$$m = 8.93 \quad \sigma_r^* = 1334\ \text{MPa}. \tag{13}$$

VI. Application of the Model to a Fatigue Specimen

The damage-mechanics-based fatigue model is applied to a dog-bone-shaped fatigue specimen to predict the stress–life behavior and to investigate the influence of various material parameters and process-induced material flaws on fatigue scatter. Fig. 6 shows the dimensions of the simulated specimen. Specimens of similar shape and dimension have been produced using micromachining techniques by several research groups [28]–[31] for fatigue testing by external actuation. Table I contains the parameters used in this investigation. Fifty material

TABLE I
SIMULATION PARAMETERS

Elastic modulus of material (E)	175 GPa
Poisson's ratio ν	0.31
Tensile Strength	550 MPa
Mean Element size	13 μm
Damage increment (ΔD)	0.02
Stress amplitude σ_a	200 MPa
Stress ratio R = $\sigma_{\max}/\sigma_{\min}$	-1

domains were generated using the Voronoi tessellation process to evaluate the statistical nature of the fatigue phenomena. The boundary conditions imposed on the specimen are that the x displacement degrees of freedom on one end are fixed while the x displacement degrees of freedom on the other end are specified such that the desired stress amplitude is obtained in the straight section of the specimen. It is assumed that the fatigue behavior is governed by the normal stress component acting on the element boundaries. To reduce the computational effort for the statistical and stress–life investigations of the tensile specimen, the simulations were performed only up to the condition of crack initiation. This is warranted in light of the fact that much of the scatter that occurs in fatigue data can be attributed to the initiation and early growth of fatigue cracks [23] and also due to the fact that, in the case of high-cycle fatigue, much of the life is spent in the crack initiation stage [32].

Shown alongside the experimental data and curve fit in Fig. 5 are the analytical results obtained using the model under the assumption of uniform material properties (E, ν, σ_r, and m). At each stress level, simulations were performed using ten domains. Under the assumption of uniform material properties, the only source of randomness is topological randomness due to the geometrical variations in the microstructures produced using the Voronoi tessellation process. As can be seen from Fig. 5, this source of randomness alone has very little effect on the scatter in the fatigue data. Note, however, that there is good agreement between the simulated and experimental results.

VII. EFFECT OF MATERIAL INHOMOGENEITY ON FATIGUE LIFE

Inhomogeneous material behavior can result from geometrical variations in the microstructure, grain anisotropy, and spatially distributed material properties. To investigate the effects of material inhomogeneity on fatigue life, three sources will be considered independently. The conditions to be investigated are geometrical variations, variable elastic modulus, and variable resistance stress. For each condition, 50 domains are subjected to a maximum stress of 200 MPa under completely reversed loading conditions until a crack initiates.

A. Geometrical Variations

In this case, the material elastic and damage properties (E, ν, σ_r, and m) are held constant throughout the domain. This condition isolates the variability between the domains to that of the randomness of the microstructural boundaries that occurs as a result of the Voronoi tessellation process. The results for this condition are shown on a Weibull probability plot in Fig. 7. The Weibull slope is 12.94, and the Weibull strength, indicating the number of cycles for which the probability of failure is 63.2%, is 2.6 (million cycles).

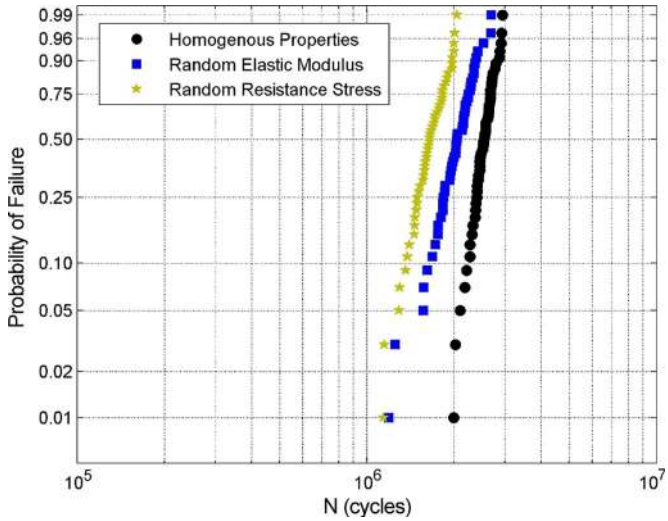

Fig. 7. Weibull life plot for crack initiation in 50 different domains subjected to different material property conditions.

B. Variable Elastic Modulus

For the second condition, the elastic modulus is assumed to vary spatially throughout the domain. This condition is implemented by treating the elastic modulus as a random variable and sampling each of the individual joint stiffnesses K_n and K_t from a normal distribution centered at a mean modulus of 175 GPa and with a standard deviation of 5.83 GPa. The other material properties (ν, σ_r, and m) are held constant. This condition will create local stress concentrations in the domain due to the interaction of elements with different stiffnesses. The results are shown in Fig. 7. The data fall in a straight line, indicating adherence to a Weibull distribution. The Weibull slope of the data is 7.61, and the Weibull strength is 2.2 (million cycles). The lower values of the Weibull slope and Weibull strength indicate an increase in scatter and a reduction in the fatigue life as compared with the homogenous property condition.

C. Variable Resistance Stress

For the final condition, a spatially distributed value of resistance stress σ_r is considered. This condition is implemented in the model by sampling the resistance stress term for each interelement joint from a normal distribution with a mean of 1334 MPa and a standard deviation of 89 MPa. The other material properties (E, ν, and m) are held constant. The results for this condition are also shown in Fig. 7. Again, the data follows a straight line. The Weibull slope of the data is 8.58, and the Weibull strength is 1.8 (million cycles). This condition leads to a nearly identical increase in scatter as was found for the variable elastic modulus condition. As expected, a larger

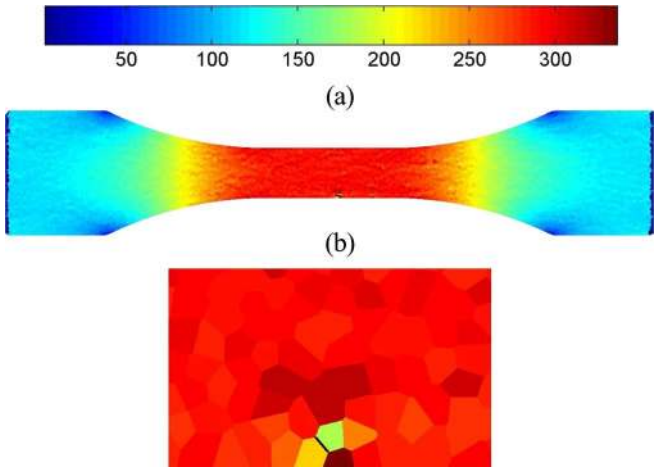

Fig. 8. (a) Von Mises stress distribution in a tensile specimen with one initially broken bond for a stress amplitude of 300 MPa. (b) Close-up view of the stress distribution around the initially broken bond represented by the black line. The stress values are given in megapascals.

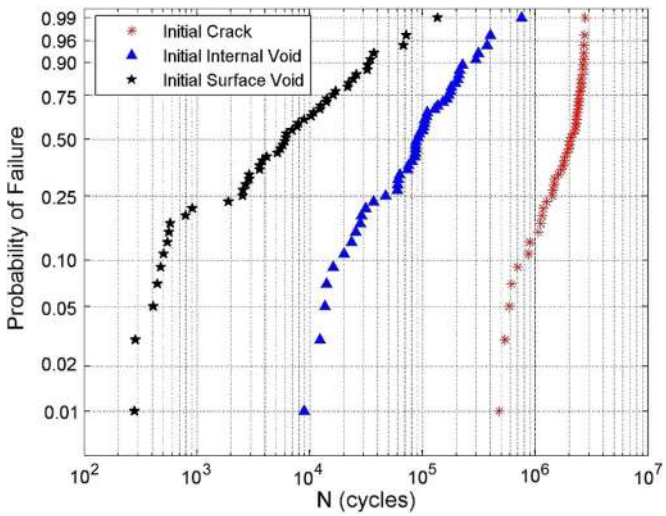

Fig. 9. Weibull life plot for crack initiation in 50 different domains with initial flaws.

reduction in fatigue life results for this condition, because the resistance stress variable relates directly to the fatigue strength of the elements.

VIII. Effect of Material Flaws on Fatigue Life

Flaws in MEMS components can be produced both during fabrication and postprocessing. During fabrication, voids and/or weak bonds can form between neighboring grains. During etching processes, overetch can lead to undercuts and/or surface flaws. For the case of polysilicon material, work has been conducted to characterize the critical flaw size and location in the context of brittle failure [33]–[36]. These same flaw populations can act as sites of stress concentration where fatigue crack initiation is likely to occur. In this section, the effects of three types of initial material flaws on fatigue life are considered. For each type of flaw, life data were obtained for 50 domains under the loading conditions considered previously.

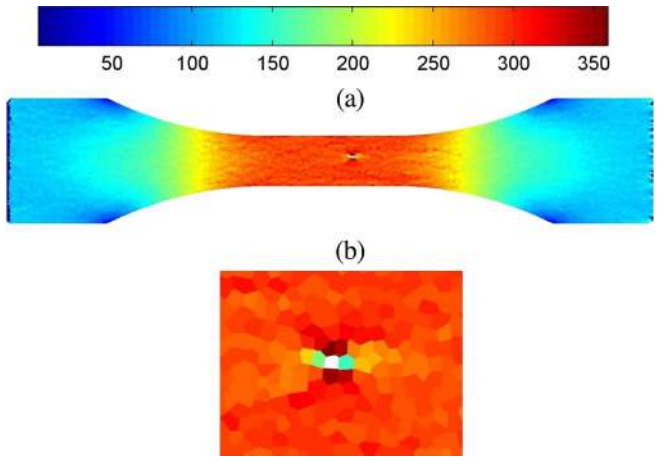

Fig. 10. (a) Von Mises stress distribution in a tensile specimen with one initial internal void for a stress amplitude of 300 MPa. (b) Close-up view of the stress distribution around the void. The stress values are given in megapascals.

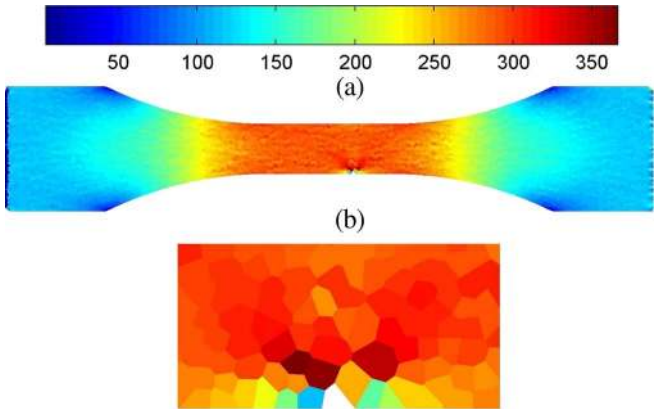

Fig. 11. (a) Von Mises stress distribution for a tensile specimen with one initial surface void for a stress amplitude of 300 MPa. (b) Close-up view of the stress distribution around the initial surface void. The stress values are given in megapascals.

A. Initially Broken Intergranular Bond

The first type of flaw considered was an initially broken intergranular bond. This flaw is implemented in the model by randomly selecting a joint within the straight section of the dog bone and assigning it an initial damage value of one. A joint with a damage value of one will have no stiffness in tension and a reduced stiffness in compression over that of the surrounding material. Uniform material properties are assumed. The distribution of Von Mises stress around an initially broken bond, represented by a black line, for one of the specimens is shown in Fig. 8. The stress concentration caused by the flaw can be clearly seen in Fig. 8. The crack initiation lives are shown on a Weibull probability plot in Fig. 9. The Weibull slope of the data is 3.21, and the Weibull strength is 2.1 (million cycles). The Weibull slope indicates a much larger increase in scatter than resulted for each of the variable material property cases. However, the Weibull strength falls between those that resulted for the conditions of variable elastic modulus and variable resistance stress.

TABLE II
WEIBULL PROBABILITY STATISTICS

Simulation Condition	Weibull Slope, e	Weibull Strength (cycles)
Homogenous	12.94	2626567
Variable Modulus	7.61	2173140
Variable Resistance Stress	8.58	1755693
Initial broken intergranular bond	3.21	2125316
Initial internal void	1.12	133009
Initial surface void	0.71	11266

B. Internal Void

The second type of flaw considered was an internal void within the domain. This is implemented in the model by randomly removing one element from the interior of straight section of each domain. The distribution of Von Mises stress around the internal void for one of the domains is shown in Fig. 10. The crack initiation lives are shown on a Weibull probability plot in Fig. 9. The Weibull slope of the data is 1.12, and the Weibull strength is 133 000 (cycles). This condition leads to a large increase in scatter and to a large decrease in the Weibull strength.

C. Surface Void

The final type of material flaw that will be considered is an initial surface void as might result from nonperfect wet or dry etching [37]. This is implemented in the model by randomly removing one element from the surface of the straight section of each specimen. The distribution of Von Mises stress around a surface void for one of the domains is shown in Fig. 11. The crack initiation lives are shown on a Weibull probability plot in Fig. 9. The Weibull slope of the data is 0.71, and the Weibull strength is 11 266 (cycles). This condition leads to the largest increase in scatter and largest decrease in Weibull strength of all the conditions considered.

The Weibull statistics for all of the material property and flaw cases are summarized in Table II. Material property variation led to a slight increase in scatter and also to a slight decrease in the Weibull strength. The results were similar for both the variable elastic modulus and variable resistance stress conditions. The initially broken intergranular bond condition led to a larger increase in scatter but to a decrease in Weibull strength that was similar to the variable material property conditions. The most critical effects were seen for the initial internal and surface voids which both led to a large reduction in the Weibull strength indicating a significantly lower fatigue life. Please note that for the material flaw cases, particularly the initial surface void case, the results do not follow a straight line, indicating that the two-parameter Weibull distribution is not the best fit and perhaps another distribution should be considered.

IX. EFFECT OF MATERIAL FLAWS ON STRESS–LIFE BEHAVIOR

The previous simulations have all been performed at a single stress level so that some characteristics of the statistical behavior could be described. Also of interest to the MEMS designer is the fatigue behavior of a component over a range of stresses. To capture this behavior, simulations are performed at five different stress levels so that a stress–life curve can be obtained. Three stress–life results are produced corresponding to each of the three types of initial flaws considered previously. For each initial flaw condition, ten domains with uniform material properties were used at each stress level. As was shown in Figs. 8, 10, and 11, each type of initial flaw led to a stress concentration in the domain. Depending upon the stress level and the severity of the stress concentration, static failure could occur. To check for static failure, the normal stress in each joint is first compared against the static strength of the material, listed in Table I, before the damage evolution equation is applied. If the stress in any joint exceeds the tensile strength of the material, the joint is assumed to break under static conditions.

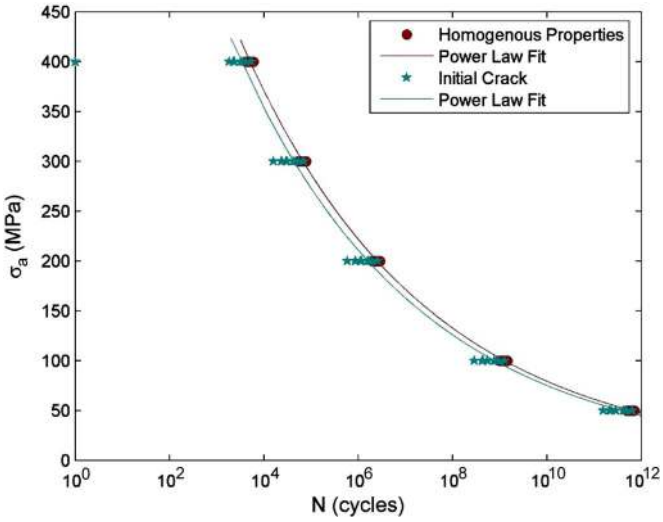

Fig. 12. S–N curve for crack initiation in a tensile specimen with one initially broken bond.

The stress–life results corresponding to each of the initial flaw conditions are shown in Figs. 12–14. Also shown for comparison purposes are the stress–life results for the ten domains used for each condition in the absence of the flaw considered. Fig. 12 shows the stress–life curve for the initially broken intergranular bond. The data follow very closely the flaw-free condition with some overlap in the data occurring at each stress level. At the highest stress level, 400 MPa, two of the domains failed statically. Fig. 13 shows the stress–life results for the case of an initial internal void. Much more scatter can be seen in the data compared to the initially broken bond

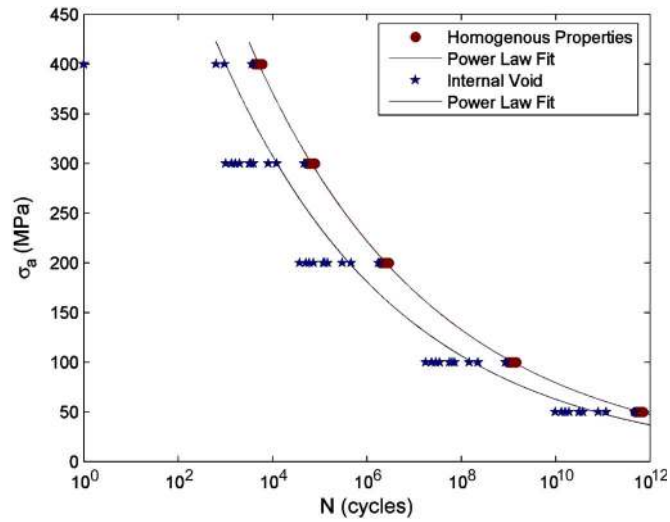

Fig. 13. S–N curve for crack initiation in a tensile specimen with one initial internal void.

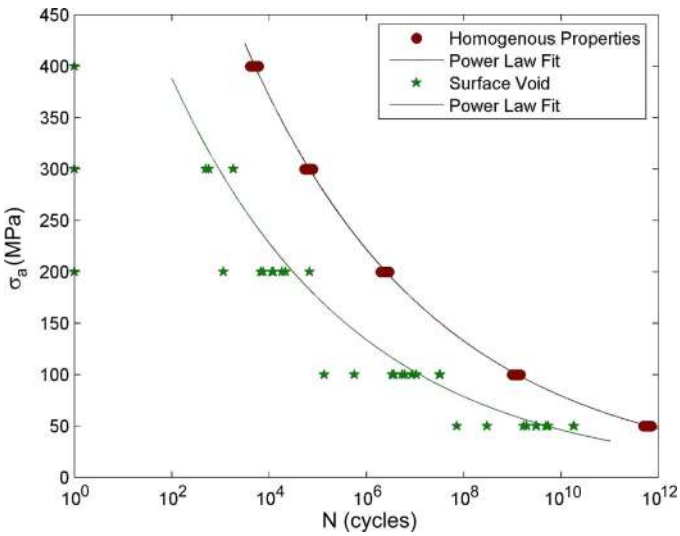

Fig. 14. S–N curve for crack initiation in a tensile specimen with one initial surface void.

case. At the highest stress level, seven of the domains failed statically. Fig. 14 shows the stress–life results corresponding to the condition of an initial surface void. This condition led to the largest increase in scatter, the largest decrease in life, and to the most domains failing statically. At the highest stress level, all ten domains failed statically. At a stress of 300 MPa, six of the domains failed statically, and at a stress of 200 MPa, one domain failed statically.

For each of the stress–life results developed, a power law fit is made through the mean of the life data that did not fail statically at each stress level. For each condition, the slope of the power law curve was within 5% of that of that given for the experimental data in (10). The results indicate the deleterious effects caused by the initial flows which lead to both a reduction in the overall life and to an increase in scatter in the data. For the surface void condition, the fatigue life at the lower stress levels is spread out over more than two orders of magnitude of cycles.

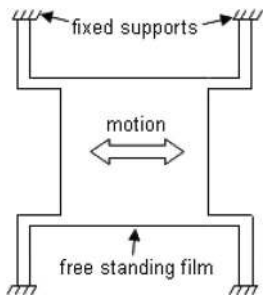

Fig. 15. MEMS resonator.

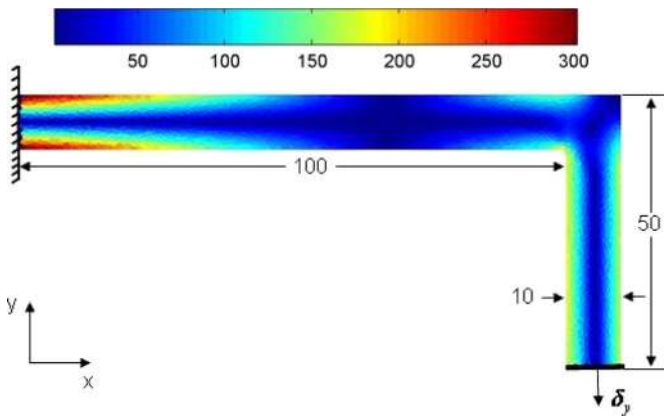

Fig. 16. Von Mises stress distribution in a MEMS resonator support beam subjected to $\delta_y = 1.0$ μm displacement. Dimensions are in micrometers. The stress values are given in megapascals.

X. Predicting the Life of a MEMS Resonator

The previous simulations were performed for the simple stress state of cyclic uniform tension/compression. MEMS structures are varied and are subjected to many different states of stress. One common structure, as shown in Fig. 15, consists of a membrane suspended above a substrate by supporting beams. Such a structure might be found in application as a MEMS resonator, variable capacitor, or accelerometer [38]–[40]. Simulations were performed to determine the life of one of the supporting beams as it is subjected to cyclically varying loads due to the motion of the membrane. The material properties listed in Table I will again be used. The dimensions of the supporting beam are shown in Fig. 16. The boundary conditions imposed on the beam are that one end is fixed while, at the other end, all of the elements are given an equivalent displacement in the y-direction. The distribution of Von Mises stress that is developed in the beam due to these boundary conditions is shown in Fig. 16. Bending stresses are developed in both the horizontal and vertical sections of the beam with the maximum stresses occurring at the fixed end. To produce a stress–life curve, simulations were performed at four different displacement amplitudes from 1.0 to 0.25 (μm). The simulations are performed through both the crack initiation and crack propagation stages so that the total life of the beam is obtained. The life of a particular beam versus the number of broken joints in the domain is shown in Fig. 17. It can be seen in the figure that, at a certain number of cycles, a large number of joints break at once. This is the point at which

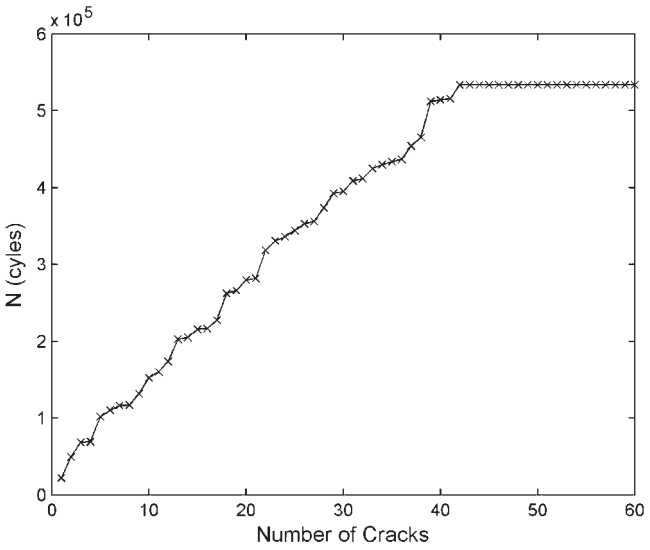

Fig. 17. Fatigue life versus the number of cracks in the beam supporting structure for a particular domain.

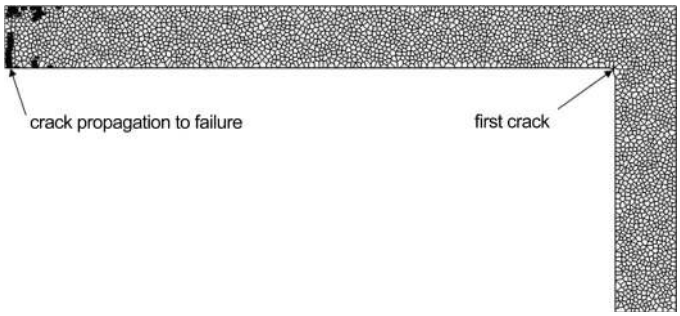

Fig. 18. Crack propagation pattern in MEMS resonator support beam.

catastrophic failure occurs and determines the total life of the component. The final crack pattern for the beam whose life is depicted in Fig. 17 is shown in Fig. 18. For this and many of the domains generated, the first crack to develop often occurs at the corner where the vertical and horizontal sections meet due to the stress concentration that this union creates. For all of the cases considered, the crack that propagated to failure occurred close to the fixed end. The lives of ten beams are found at each displacement amplitude. The stress versus life result is shown in Fig. 19. The stress values given along the ordinate are the maximum stresses that occur in the domain at each displacement amplitude. Note that, although the simulations were performed until the final fracture of the beam, the effective life of such a resonating component may be limited by an unacceptable shift in resonance frequency or by an inability to control the device caused by degradation of the material before it actually fractures [40].

XI. Summary and Conclusion

This paper has presented a phenomenological discrete brittle damage-mechanics-based model that can be used to evaluate the fatigue life of MEMS devices. A discrete material representation is used in which a material domain is represented by a collection of rigid elements connected by springs. The

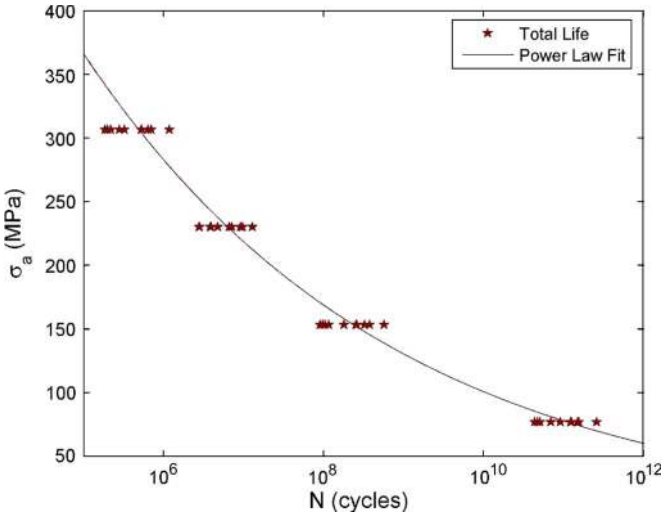

Fig. 19. S–N curve for the total life of a MEMS resonator support beam.

stiffnesses of the springs are degraded according to a continuum damage-mechanics model as the domain is subjected to fatigue loading. The material properties of the damage model can be identified from experimental stress–life results. The model can simulate the lifetime of a component from crack initiation until final fracture. Statistical variations in material properties are included by randomly assigning spring properties from a normal distribution. Through simulations of a LIGA NI fatigue specimen, it was shown how variable material properties can lead to fatigue scatter and a reduction in life. The same specimen was used to demonstrate the ability of the model to account for material flaws caused by imperfect fabrication techniques. The presence of an initial surface void was found to be the most detrimental condition. Stress–life curves generated using the model showed fatigue lives scattered over more than two orders of magnitudes of cycles for some conditions. The ability of the model to predict the lives of different types of devices and loading conditions was demonstrated by generating the stress–life curve for a LIGA-Ni-based MEMS resonator support beam.

Acknowledgment

The authors would like to thank the DARPA MEMS/NEMS S & T fundamentals program and the IMPACT Center for their support of this research project.

References

[1] K. H. L. Chau and R. E. Sulouff, "Technology for the high-volume manufacturing of integrated surface-micromachined accelerometer products," *Microelectron. J.*, vol. 29, no. 9, pp. 579–586, Sep. 1998.

[2] D. R. Sparks, S. R. Zarabadi, J. D. Johnson, Q. Jiang, M. Chia, O. Larsen, W. Higdon, and P. Castillo-Borelley, "A CMOS integrated surface micromachined angular rate sensor: It's automotive applications," in *Proc. Int. Conf. Solid-State Sens. Actuators*, 1997, vol. 2, pp. 851–854.

[3] C. L. Goldsmith, D. I. Forehand, Z. Peng, J. C. M. Hwang, and J. L. Ebel, "High-cycle life testing of RF MEMS switches," in *IEEE MTT-S Int. Microw. Symp. Dig.*, 2007, pp. 1805–1808.

[4] I. Chasiotis, "Mechanics of thin films and microdevices," *IEEE Trans. Device Mater. Rel.*, vol. 4, no. 2, pp. 176–188, Jun. 2004.

[5] C. L. Muhlstein, S. B. Brown, and R. O. Ritchie, "High-cycle fatigue of polycrystalline silicon thin films in laboratory air," in *Proc. Mater. Res. Soc. Symp.*, 2001, vol. 657, pp. EE581–EE586.

[6] H. Kahn, R. Ballarini, R. L. Mullen, and A. H. Heuer, "Electrostatically actuated failure of microfabricated polysilicon fracture mechanics specimens," *Proc. R. Soc. Lond. A, Math. Phys. Sci.*, vol. 455, no. 1990, pp. 3807–3823, Oct. 1999.
[7] H. Kapels, R. Aigner, and J. Binder, "Fracture strength and fatigue of polysilicon determined by a novel thermal actuator," *IEEE Trans. Electron Devices*, vol. 47, no. 7, pp. 1522–1528, Jul. 2000.
[8] J. Bagdahn and W. N. Sharpe, "Fatigue of polycrystalline silicon under long-term cyclic loading," *Sens. Actuators A, Phys.*, vol. 103, no. 1/2, pp. 9–15, Jan. 2003.
[9] W. N. Sharpe and J. Bagdahn, "Fatigue testing of polysilicon—A review," *Mech. Mater.*, vol. 36, no. 1/2, pp. 3–11, Jan. 2003.
[10] H. Kahn, R. Ballarini, and A. H. Heuer, "Dynamic fatigue of silicon," *Curr. Opin. Solid State Mater. Sci.*, vol. 8, no. 1, pp. 71–76, Jan. 2004.
[11] T. E. Buchheit, B. L. Boyce, and G. W. Wellman, "The role of microstructure in MEMS deformation and failure," in *Proc. IMECE*, 2002, pp. 559–566.
[12] J. Aktaa, J. T. Reszat, M. Walter, K. Bade, and K. J. Hemker, "High cycle fatigue and fracture behavior of LIGA nickel," *Scr. Mater.*, vol. 52, no. 12, pp. 1217–1221, Jun. 2005.
[13] Y. Yang, B. I. Imasogie, S. M. Allameh, B. Boyce, K. Lian, J. Lou, and W. O. Soboyejo, "Mechanisms of fatigue in LIGA Ni MEMS thin films," *Mater. Sci. Eng. A*, vol. 444, no. 1/2, pp. 39–50, Jan. 2007.
[14] B. L. Boyce, J. R. Michael, and P. G. Kotula, "Fatigue of metallic microdevices and the role of fatigue-induced surface oxides," *Acta Mater.*, vol. 52, no. 6, pp. 1609–1619, Apr. 2004.
[15] L. M. Kachanov, "Time of the rupture process under creep conditions," *Izv. Akad. Nauk SSSR, Otd. Teh. Nauk*, vol. 8, pp. 26–31, 1958.
[16] Y. N. Robotnov, *Creep Problems in Structural Mechanics*. Amsterdam, The Netherlands: North Holland, 1969.
[17] J. L. Chaboche, "Continuum damage mechanics: Part I—General concepts," *J. Appl. Mech.*, vol. 55, pp. 59–64, 1988.
[18] N. Raje, F. Sadeghi, and R. G. Rateick, Jr., "A discrete element approach to evaluate stresses due to line loading on an elastic half-space," *Comput. Mech.*, vol. 40, no. 3, pp. 513–529, Aug. 2007.
[19] A. V. Potapov, C. S. Campbell, and M. A. Hopkins, "A two-dimensional dynamic simulation of solid fracture—Part I: Description of the model," *Int. J. Mod. Phys. C*, vol. 6, no. 3, pp. 371–398, 1995.
[20] O. Ito and E. R. Fuller, "Computer modeling of anisotropic grain microstructure in two dimensions," *Acta Metall. Mater.*, vol. 41, no. 1, pp. 191–198, Jan. 1993.
[21] P. D. Zavattieri and H. D. Espinosa, "Grain level analysis of crack initiation and propagation in brittle materials," *Acta Mater.*, vol. 49, no. 20, pp. 4291–4311, Dec. 2001.
[22] J. Lemaitre, *A Course on Damage Mechanics*. Berlin, Germany: Springer-Verlag, 1992.
[23] V. V. Bolotin and I. L. Belousov, "Early fatigue crack growth as the damage accumulation process," *Probabilistic Eng. Mech.*, vol. 16, no. 4, pp. 279–287, Oct. 2001.
[24] J. L. Chaboche and P. M. Lesne, "A non-linear continuous fatigue damage model," *Fatigue Fract. Eng. Mater. Struct.*, vol. 11, no. 1, pp. 1–17, Jan. 1988.
[25] Y. C. Xiao, S. Li, and Z. Gao, "A continuum damage mechanics model for high cycle fatigue," *Int. J. Fatigue*, vol. 20, no. 7, pp. 503–508, Aug. 1998.
[26] I. Rasool Memon, X. Zhang, and D. Cui, "Fatigue life prediction of 3-D problems by damage mechanics with two-block loading," *Int. J. Fatigue*, vol. 24, no. 1, pp. 29–37, Jan. 2002.
[27] V. V. Bolotin, *Mechanics of Fatigue*. Boca Raton, FL: CRC Press, 1999.
[28] J. Bagdahn and W. N. Sharpe, "Fatigue of polycrystalline silicon under long-term cyclic loading," *Sens. Actuators A, Phys.*, vol. 103, no. 1/2, pp. 9–15, Jan. 2003.
[29] S. M. Allameh, J. Lou, F. Kavishe, T. Buchheit, and W. O. Soboyejo, "An investigation of fatigue in LIGA Ni MEMS thin films," *Mater. Sci. Eng. A*, vol. 371, no. 1/2, pp. 256–266, Apr. 2004.
[30] S.-W. Kim, C.-S. Oh, and H.-J. Lee, "Specimen aligning techniques in tensile and fatigue tests for thin films," *Fatigue Fract. Eng. Mater. Struct.*, vol. 30, no. 1, pp. 64–71, Jan. 2006.
[31] J. H. Park, S. H. Choa, H. C. Choi, M. S. Myung, C. S. Lee, and Y. J. Kim, "Fatigue test of Al-3% TI using axial loading testing machine for MEMS materials," in *Proc. IPACK*, 2005, pp. 1725–1730.
[32] W. D. Callister, *Materials Science and Engineering an Introduction*. New York: Wiley, 2000.
[33] A. McCarty and I. Chasiotis, "Description of brittle failure of non-uniform MEMS geometries," *Thin Solid Films*, vol. 515, no. 6, pp. 3267–3276, Feb. 2007.
[34] D. C. Miller, B. L. Boyce, M. T. Dugger, T. E. Buchheit, and K. Gall, "Characteristics of a commercially available silicon-on-insulator MEMS material," *Sens. Actuators A, Phys.*, vol. 138, no. 1, pp. 130–144, Jul. 2007.
[35] T. E. Buchheit, S. J. Glass, J. R. Sullivan, S. S. Mani, D. A. Lavan, T. A. Friedmann, and R. Janek, "Micromechanical testing of MEMS materials," *J. Mater. Sci.*, vol. 38, no. 20, pp. 4081–4086, Oct. 2003.
[36] D. A. LaVan, B. L. Boyce, and T. E. Buchheit, "Size and frequency of defects in silicon MEMS," in *Proc. IMECE*, 2002, pp. 573–576.
[37] M. J. Madou, *Fundamentals of Microfabrication: The Science of Miniaturization*, 2nd ed. Boca Raton, FL: CRC Press, 2002.
[38] G. M. Rebeiz, *RF MEMS: Theory, Design, and Technology*. New York: Wiley-Interscience, 2002.
[39] S. S. Senturia, *Microsystem Design*, 2nd ed. New York: Springer-Verlag, 2004.
[40] D. R. Sparks, M. I. Chia, and G. Q. Jiang, "Cyclic fatigue and creep of electroformed micromachines," *Sens. Actuators A, Phys.*, vol. 95, no. 1, pp. 61–68, Dec. 2001.

Trevor S. Slack received the B.S. degree in mechanical engineering from North Carolina State University, Raleigh, and the M.S. degree in mechanical engineering from Purdue University, West Lafayette, IN, where he is currently working toward the Ph.D. degree in the Department of Mechanical Engineering.

Farshid Sadeghi is a Professor of mechanical engineering at Purdue University, West Lafayette, IN. He has authored or coauthored more than 90 archival publications in leading international journals and has given over 250 presentations at various conferences, industries, and governmental agencies. He has graduated 55 Ph.D. and M.S. students. He is currently serving as the Chairman of 12 Ph.D. and 1 M.S. students. His research interests include tribology, fatigue, fracture surface science, and microelectromechanical sensors for tribological applications.

Prof. Sadeghi is a Fellow of the American Society of Mechanical Engineers (ASME) and the Society of Tribologists and Lubrication Engineers (STLE). He was a recipient of numerous awards from the ASME and the STLE. He has chaired, cochaired, and/or organized over 75 sessions at international conferences. He served as the Chairman of the 2000 ASME Tribology Conference in Seattle, WA.

Dimitrios Peroulis received the Ph.D. degree in electrical engineering from the University of Michigan, Ann Arbor, in 2003.

Since August 2003, he has been with Purdue University, West Lafayette, IN, where he is currently leading a group of 15 Ph.D. students in a variety of research projects in the areas of MEMS for RF, sensing, and power harvesting applications, as well as RFID sensors for the health monitoring of sensitive equipment. He has nine years of experience in his field of expertise and has led a variety of projects that were funded by the Air Force, the Army, and the Defense Advanced Research Projects Agency (DARPA) in these areas. He is currently leading two DARPA projects at Purdue University focusing on: 1) very high quality ($Q > 1000$) RF tunable filters (evanescent filter cavities for analog spectral processing) and 2) developing sophisticated models for understanding the failure mechanisms of MEMS devices (University Center on MEMS/NEMS S&T Fundamentals Program). In addition, he is leading an Air Force project on RFID MEMS sensors and two National Science Foundation projects on wireless networks. He has over 40 refereed journal and conference publications in the areas of microwave integrated circuits and antennas.

Dr. Peroulis was a recipient of two Student Paper Awards at the 2001 and 2002 International Microwave Symposia, and of six Outstanding Teacher Awards at Purdue University. He is a member of the Center of Wireless Systems and Applications and the Birck Nanotechnology Center at Purdue University.